Environmental high-energy astrophysics in the context of space missions as LISA, Solar Orbiter and JWST, and its implications for space weather science

Catia Grimani

University of Urbino Carlo Bo
INFN, Italy

Raphael (Raffaello Sanzio)
1483-1520

1506 UNIVERSITÀ DEGLI STUDI DI URBINO CARLO BO

INFN
Istituto Nazionale di Fisica Nucleare

©FotoPaoloMini

Contents

- Antimatter search in cosmic rays: pulsars as most plausible astrophysical sources of high-energy positrons in cosmic rays

- Cosmic-ray role in limiting the performance of space experiments (LISA Pathfinder, LISA, Solar Orbiter): instrument diagnostics and space weather science

- Circumpulsar (magnetar) disc formation and positron measurements near Earth: clues from JWST observations and gravitational wave detection

- Conclusions

C. Grimani - Women Physicists

The discovery of cosmic rays

- 1912 cosmic-ray discovery by
  Victor F. Hess

- What are cosmic rays made of?
- Photons? No
- Energetic positively charged
  particles (protons and ions)!
  Latitude effect and east-west
  asymmetry
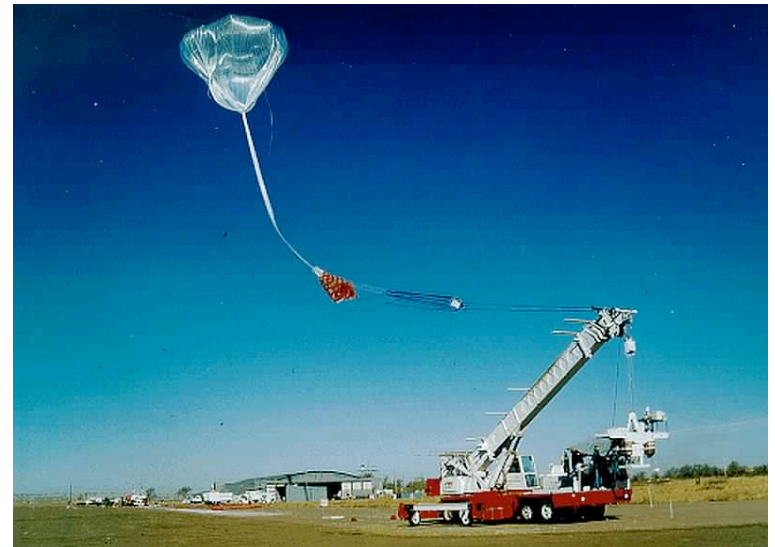- 1000 particles $m^{-2} s^{-1}$ at the top of
  the atmosphere
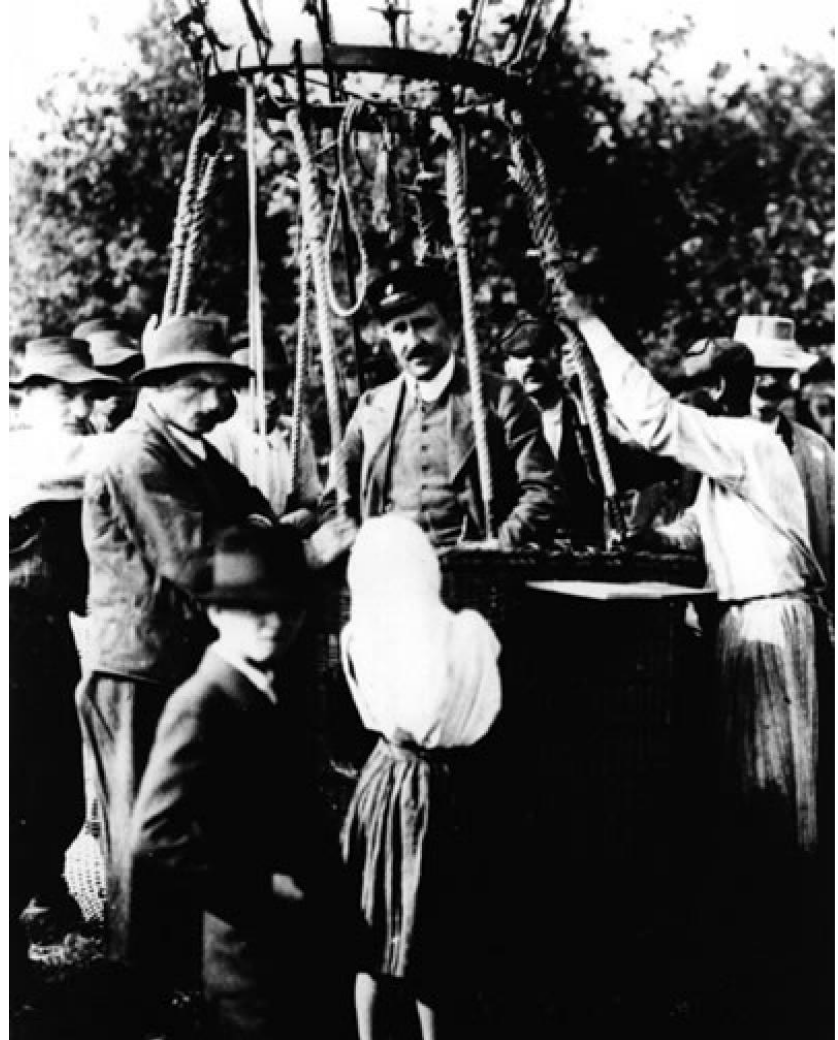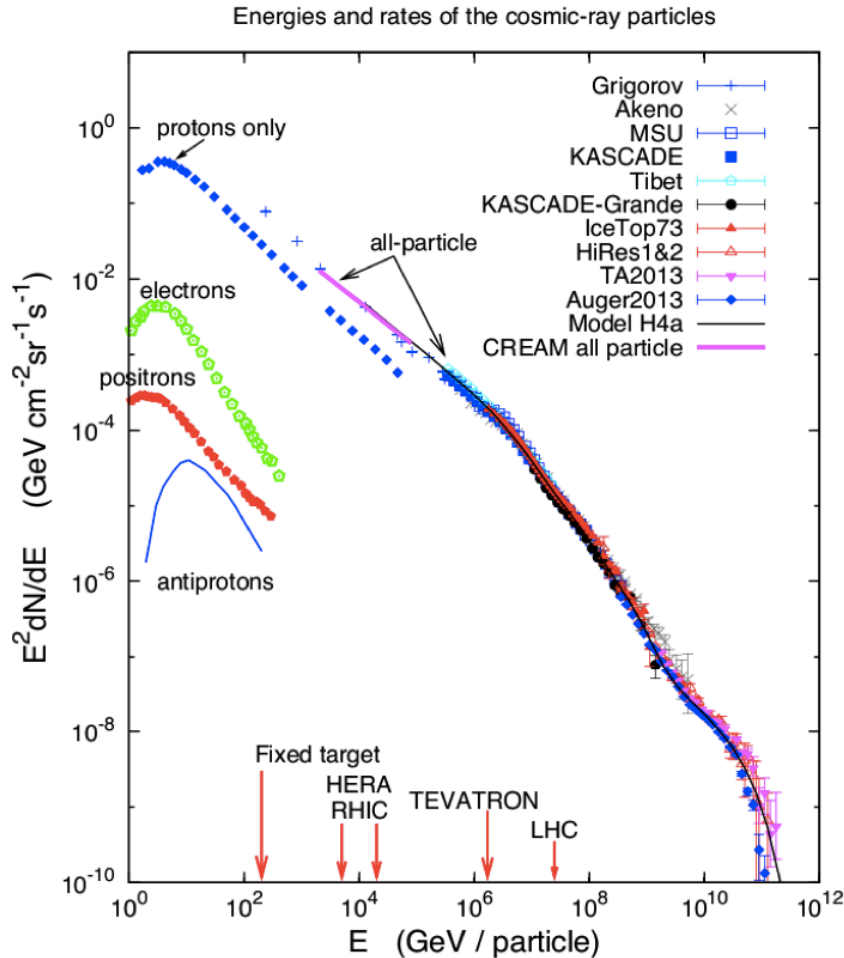
Cosmic-ray research@ NMSU 1990-1992

NSBF, NASA

Fort Sumner
NM, USA

Cosmic-ray energy spectra

Blasi, 2012

Energies and rates of the cosmic-ray particles

The cosmic-ray differential flux varies by 32 orders of magnitude when the energy varies by 12 orders of magnitude

$F(E)=A\,(E+b)^{-\alpha}\,E^{\beta}$
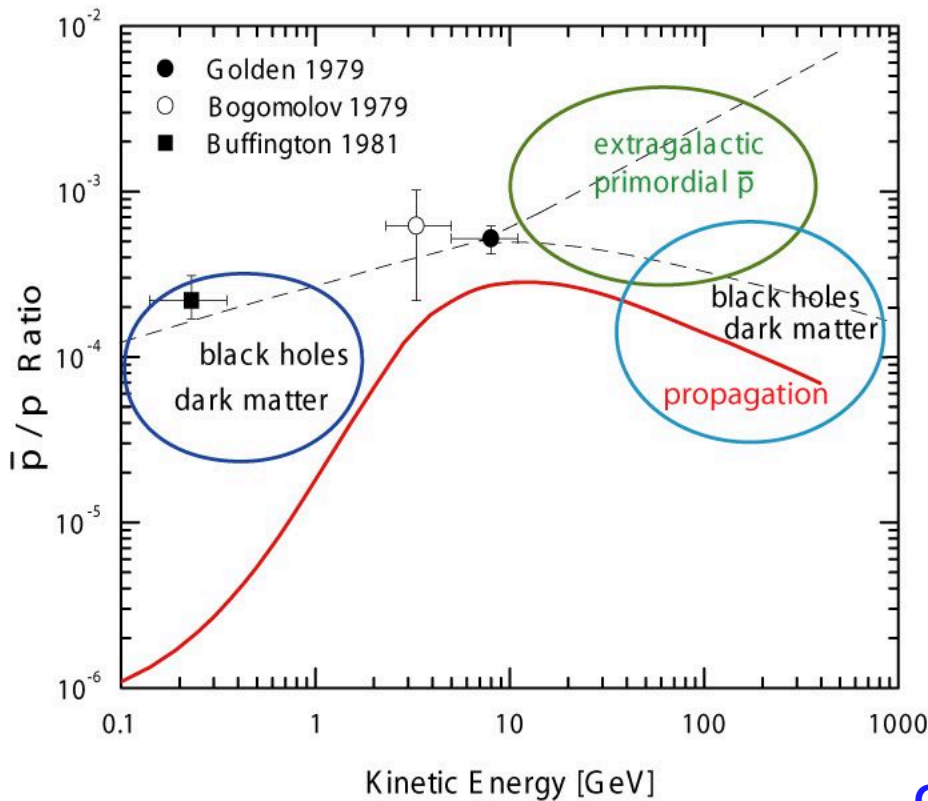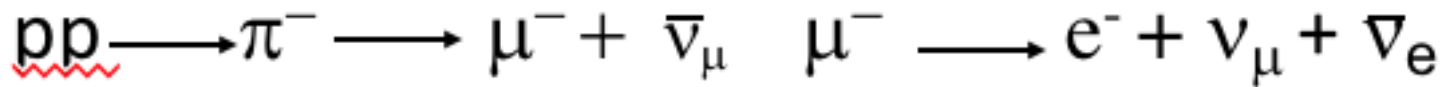particles/(m² sr s GeV)
E<100 GeV(/n)

$F(E)=A\,E^{-\gamma}$
particles/(m² sr s GeV)
E>100 GeV(/n)
with changing γ

γ = 2.7 up to the knee (3×10^{15} eV)
γ = 3−3.15 up to 10^{18} eV
γ = 2.7 above the ankle (3×10^{18} eV)
then there is a possible cut-off

Search for antimatter in cosmic rays

- Positron discovery in cosmic rays in 1964 (De Shong et al. 1964)

- Antiproton discovery in cosmic rays in 1979 (Bogomolov et al.; 1979 and Golden et al.; 1979)

- No antinucleus detection up to present time

- Which is the origin of antimatter in cosmic rays?

- Both positrons and antiprotons are produced in primary proton interactions in the interstellar medium (1 atom hydrogen cm^{-3}, for comparison on Earth surface there are 10^{19} atoms cm^{-3}). Positrons are in excess with respect to the secondary component, while the same does not applies to antiprotons.

Antiprotons and positrons as secondary particles

$$pp \longrightarrow p + p + \bar{p} + p$$

$$pp \longrightarrow \pi^+ \longrightarrow \mu^+ + \nu_\mu \qquad \mu^+ \longrightarrow e^+ + \bar{\nu}_\mu + \nu_e$$

$$pp \longrightarrow \pi^- \longrightarrow \mu^- + \bar{\nu}_\mu \qquad \mu^- \longrightarrow e^- + \nu_\mu + \nabla_e$$
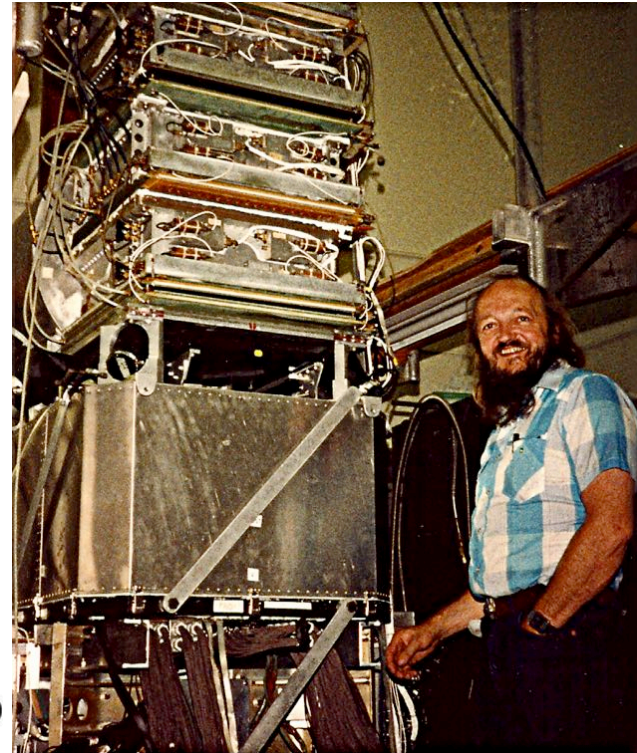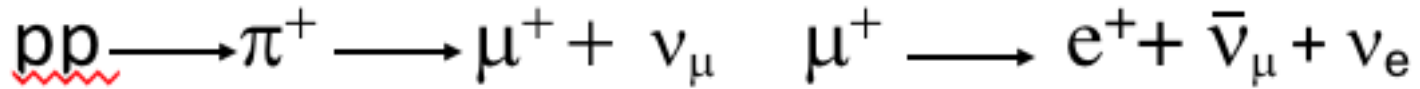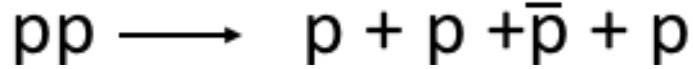
Antiproton discovery in cosmic rays in 1979

Golden et al.; 1979 and Bogomolov et al.; 1979
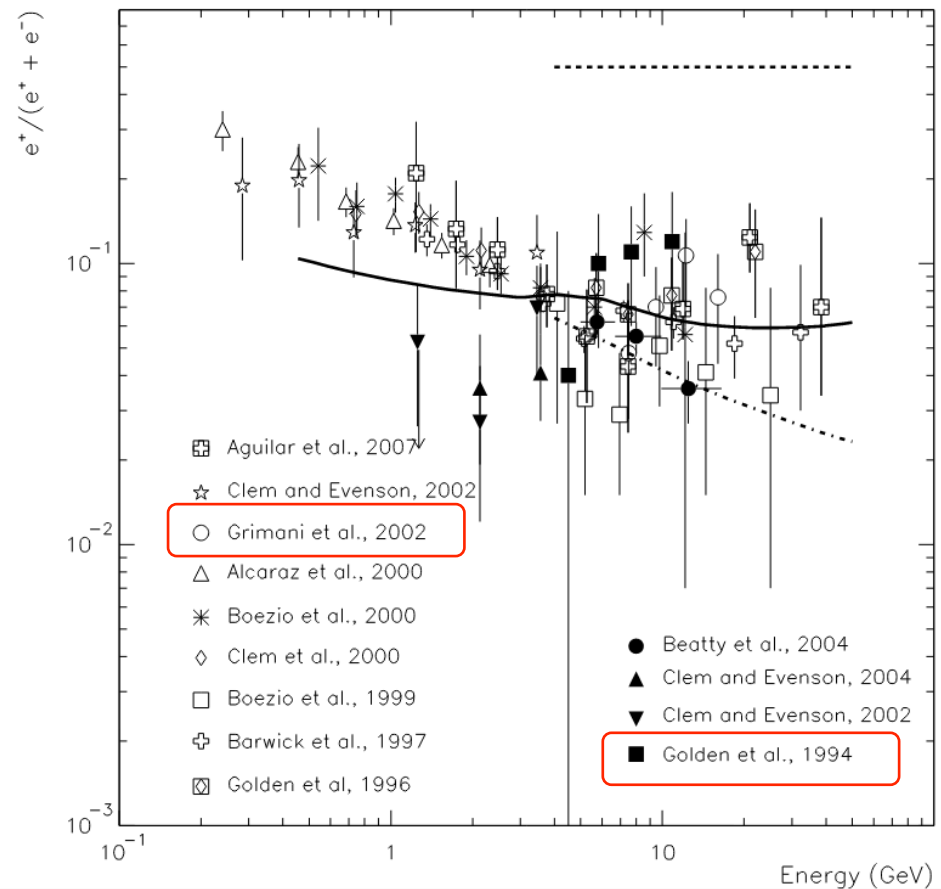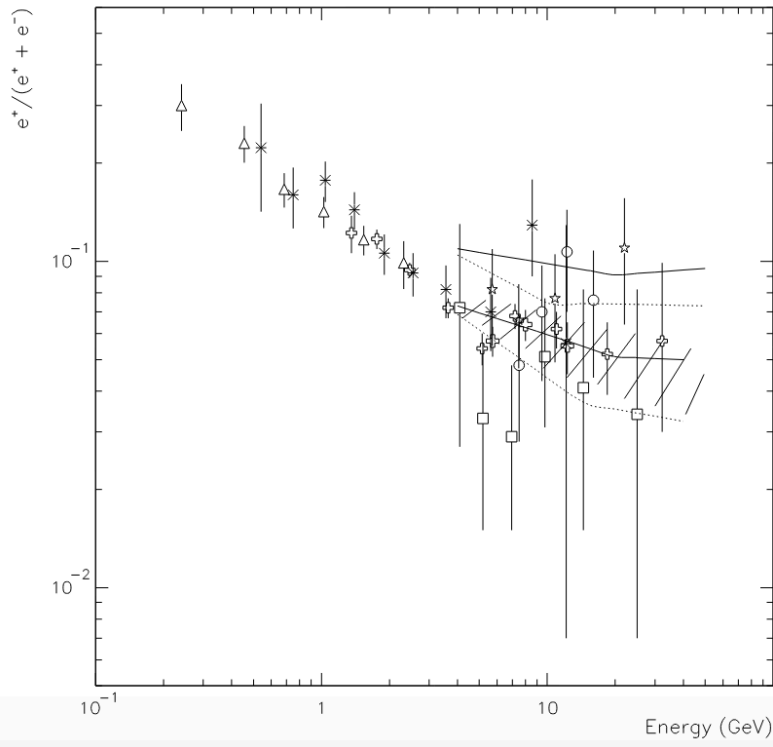
Antiproton observations in cosmic rays
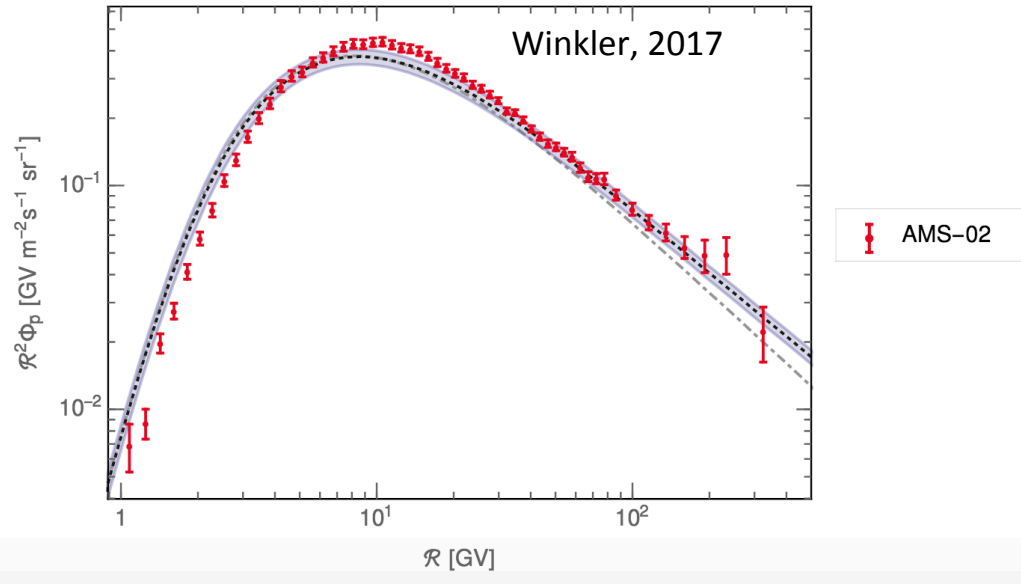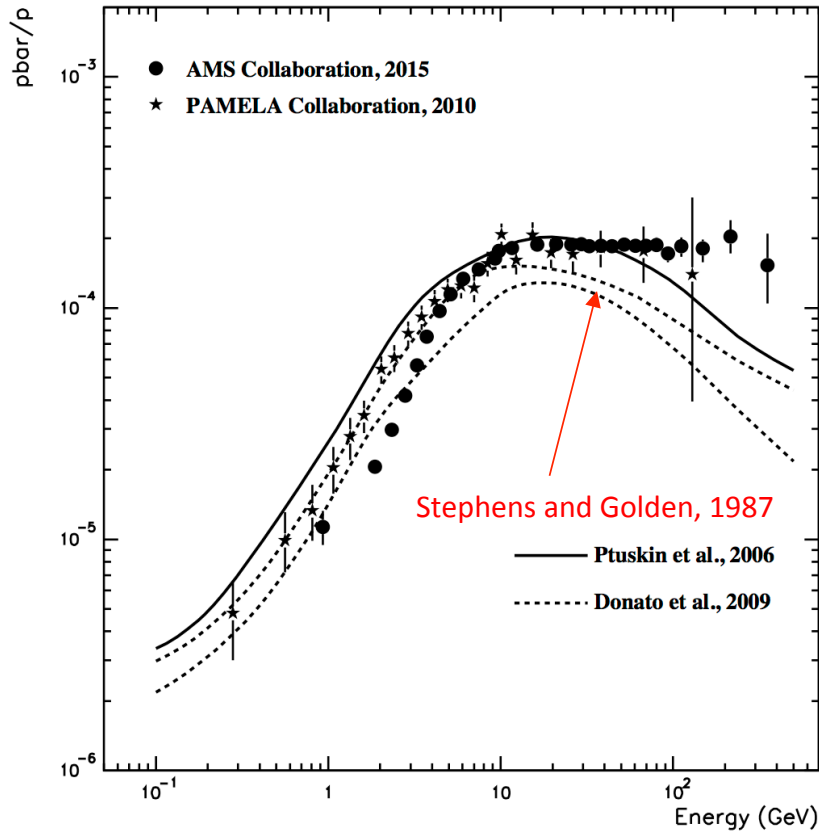
CG, Astrophysics and Space Science, 268, 465, 1999

Early positron measurements

Pulsars as astrophysical sources of high-energy positrons
Pulsar birthrate from pulsar characteristics and vice versa

Pulsar Birthrate^{-1}=200+/-100 years   Pulsar Birthrate^{-1}= 33 years

CG, A&A, 418, 649-653, 2004
CG, A&A, 474, 339-343, 2007

Positron observations in cosmic rays
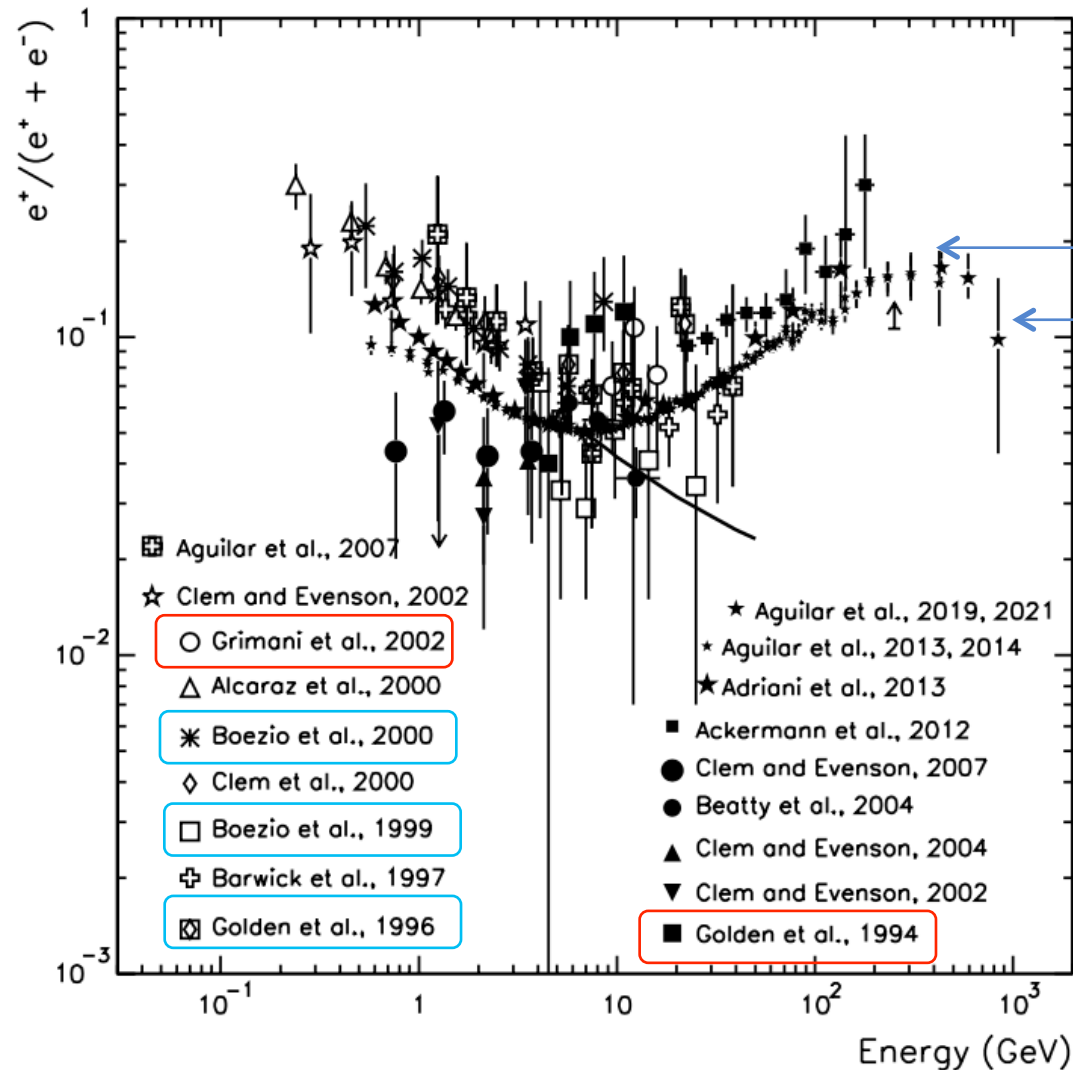
Average 7 GeV<E<50 GeV
0.064±0.003
Before PAMELA, Fermi
and AMS-01 AMS-02

284^{+91}_{-64} GeV

Cut-off 810^{+310}_{-180} GeV
Aguilar et al.; 2021
AMS-02

Positron observations are compatible with sources of TeV e^-- e^+ located between 100 and 800 pc from the Solar System (Attallah 2016).

Possible sources of positron excess

1) Primordial Black Hole Evaporation

2) ^{56}Co decay in Supernova Remnants

3) Supersymmetric particle annihilation

4) $\gamma\gamma$ interaction

5) Pulsar magnetosphere

 (Polar Cap Models- Outer Gap Models)

Bushing et al, 2007
Hooper, Blasi &
Serpico, 2009
Di Mauro et al., 2014
Feng & Zhang, 2016
CG, A&A, 2004, 2007
CG, ICRC 2015

Pulsar polar cap models

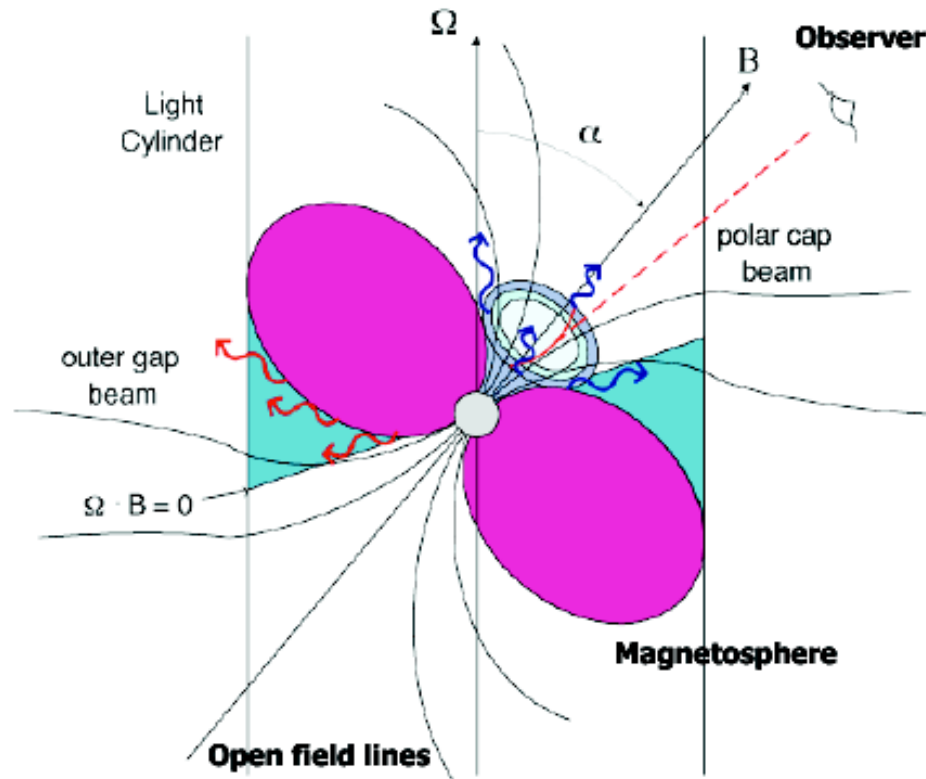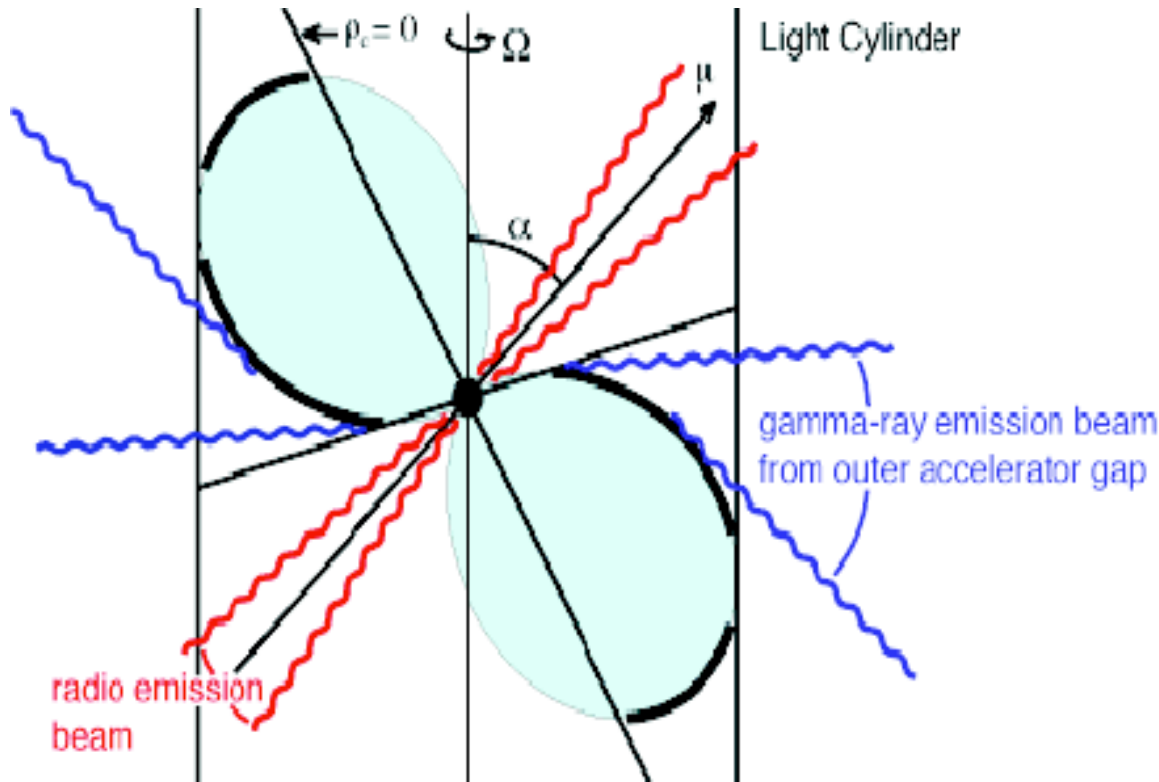Figure from http://cossc.gsfc.nasa.gov/images/epo/gallery/pulsars/

Goldreich & Julian, 1969
Harding & Ramaty, 1987

• Strong electric fields are induced by the rotating neutron star

• Electrons are extracted from the pulsar outer layer and accelerated

• Open field lines originate at polar caps ($r_{pc} = 8 \times 10^2$ m)

• Electron and positron synchrotron energy losses limit the particles to GeV energies

Pulsar outer gap models

Light Cylinder

gamma-ray emission beam
from outer accelerator gap

radio emission
beam

http://cossc.gsfc.nasa.gov/images/epo/gallery/pulsars/

Cheng, Ho & Ruderman, 1986

*Electrons are accelerated in the outer magnetosphere in vacuum gaps within a charge separated plasma
*Electrons interact through synchrotron radiation or inverse Compton scattering
*e^+e^- pairs are produced by $\gamma\gamma$ interaction

Different cut-off energies are predicted by polar cap and outer gap models for the pulsed gamma-ray spectra!

C. Grimani ECRS Florence August 31st - September 3rd 2004

Pulsar TeV pulsed gamma-ray emission

- From Crab up to 2 TeV (Ansoldi et al.; 2016)

- From Vela up to 7 TeV (Djannati-Atai et al. 2017)

- From Geminga above 20 TeV (Lopez et al. 2019)

Electron and positron Lorentz factors > 5×10^6
These evidences reveal that outer gap models are favoured over polar cap models and that pulsars are CERTAIN
sites of positron acceleration up to tens of TeV. May the pulsar environment limit the electron and positron propagation in the interstellar medium?

PHYSICS OF COSMIC RAYS FOR SPACE INSTRUMENT DIAGNOSTICS AND SPACE WEATHER SCIENCE
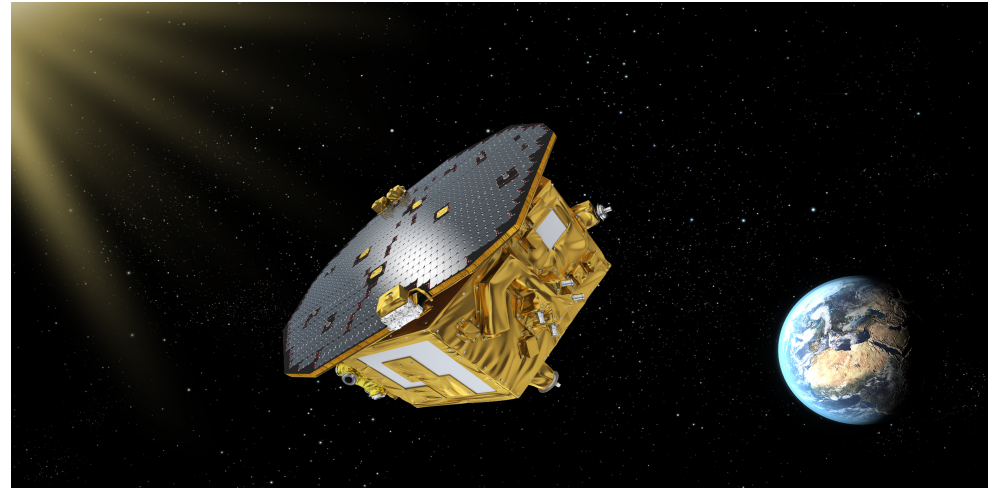
The LISA mission
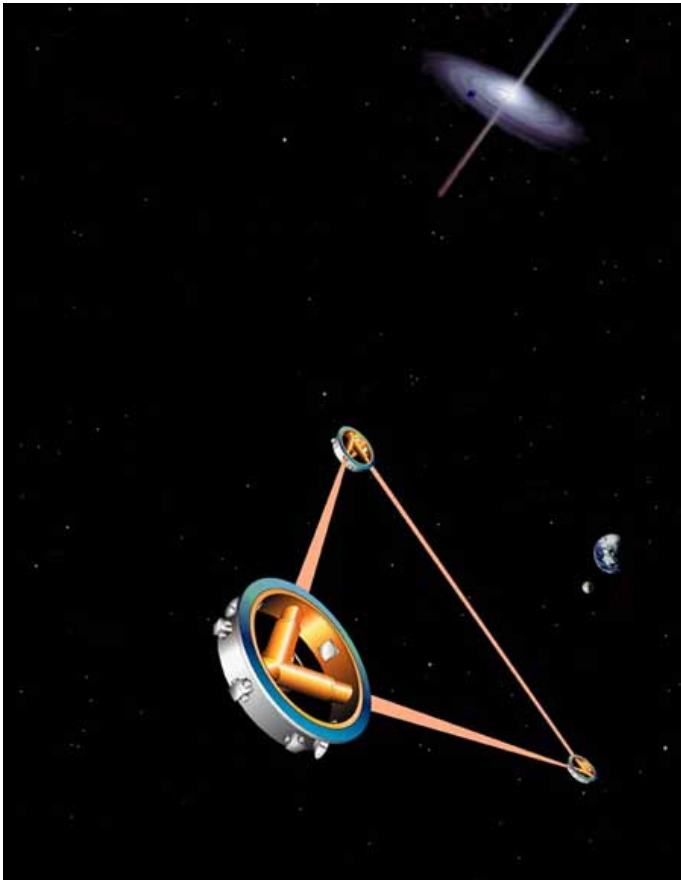
Lunch: 2035   **Arm: 2.5 10^6 km**
Orbit: Heliocentric - 3 S/C trailing
Earth at 50 million km

The LISA Pathfinder mission

Lunch: December 3, 2015 4:04 GMT
from Kourou (French Guiana)
Orbit: L1
Mission end: July 18, 2017

http://sci.esa.int/lisa-pathfinder/

https://sci.esa.int/web/lisa
https://www.elisascience.org/
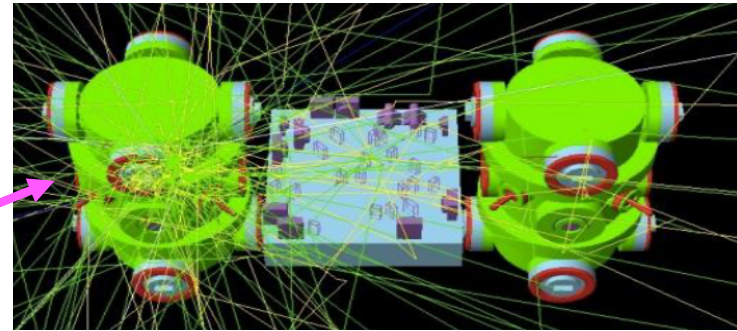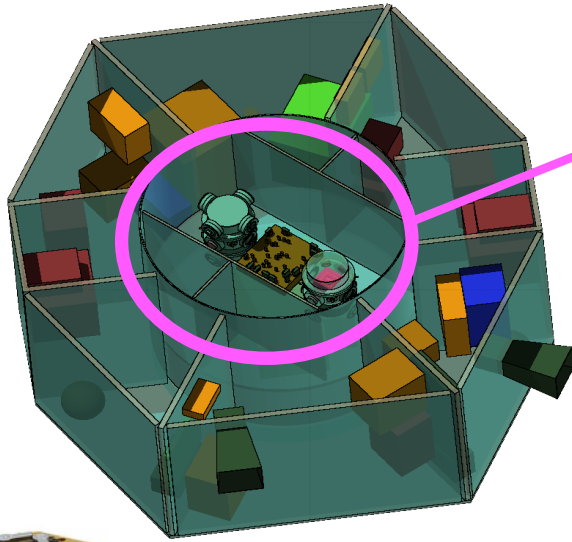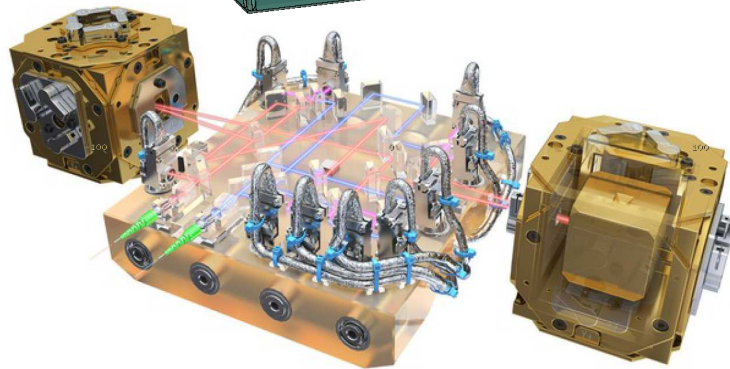
LISA Pathfinder test masses

Approximately 13 g cm^{-2} of material surrounded the test masses

Test masses:
cubes of 70% Au-30% Pt
4.6 cm side
2 kg mass
38 cm distance

Armano et al., PRL, 116, 231101, 2016
Armano et al., PRL, 120, 061101, 2018

Test-mass net and effective charging

$$\lambda_{NET} = \sum_{j=-\infty}^{+\infty} j\lambda_j$$

Ferrari et al., 2005-10 (Geneva:CERN)
Battistoni et al.,
AIP Conf. Proc. 896,
M.   Albrow and R. Raja, 31-49

$$\lambda_{EFF} = \sum_{j=-\infty}^{+\infty} j^2\lambda_j$$

$$S_Q(\omega) = \frac{S}{\omega} = \frac{\sqrt{2e^2\lambda_{eff}}}{\omega}$$

$$S = \sqrt{2e^2\lambda_{eff}} \quad e\ s^{-1}\ Hz^{-1/2}$$

Where: j is the amplitude of the charge released by each particle and λ_j is the rate of occurrence of that event.

Timeseries of the net deposited charges per particle interaction
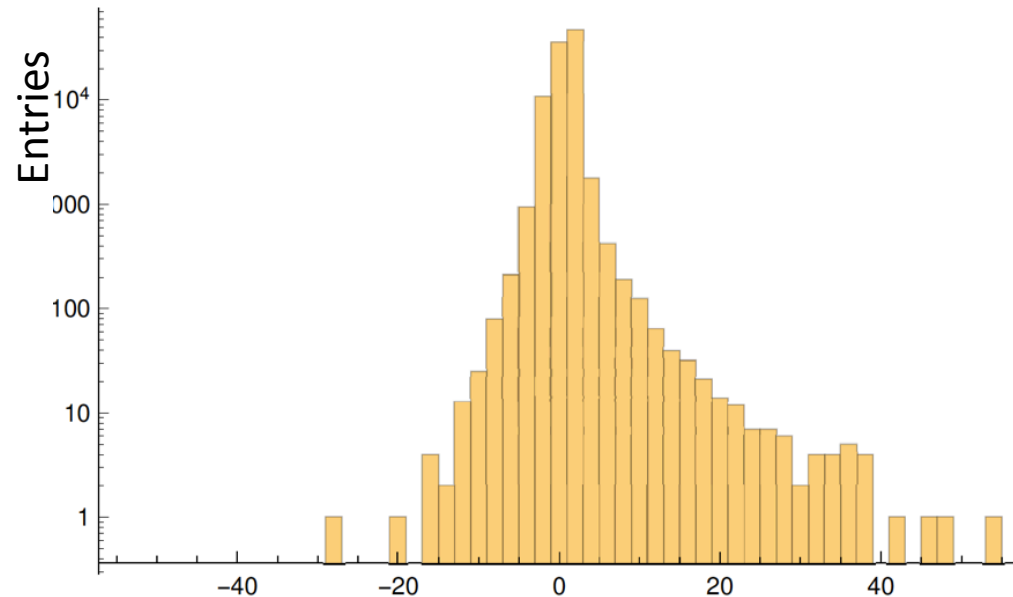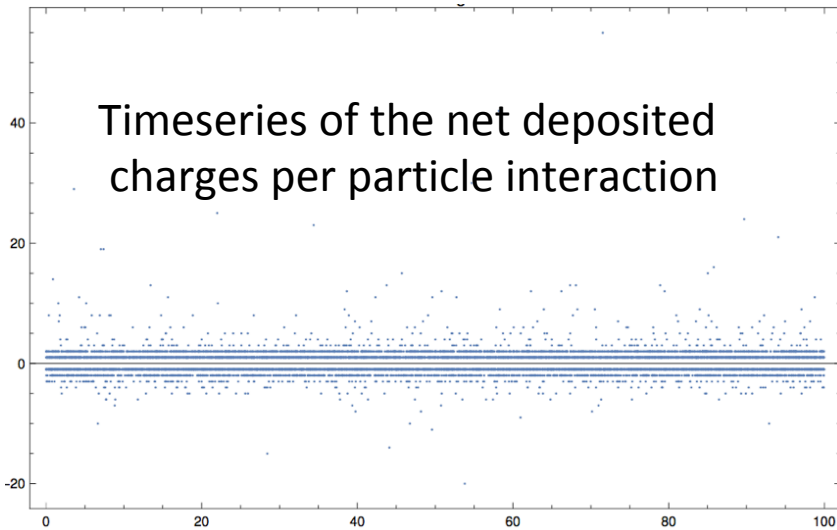
Sensitivities of future interferometers for gravitational wave detection in space
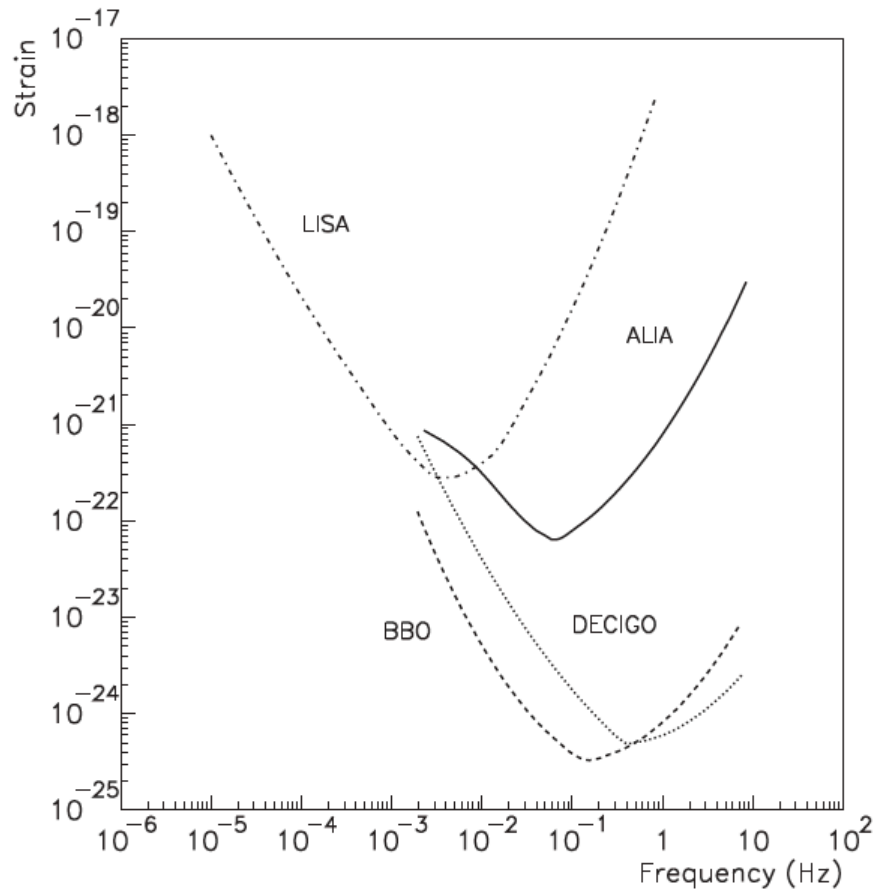
CG, MNRAS, 507 (1) , 261-266, 2021
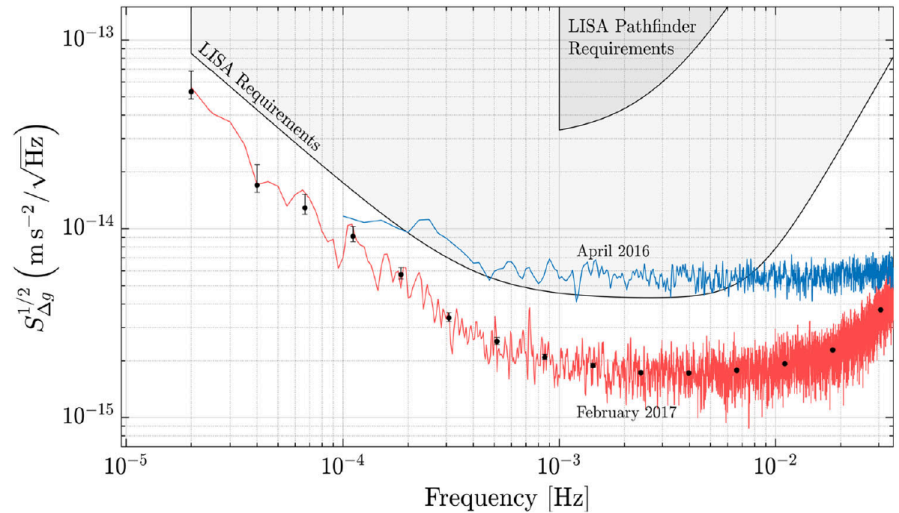
Armano et al., PRL, 120, 061101, 2018

Amplitude spectral density:
at 1.74 ± 0.01 fm s^{-2}/Hz$^{0.5}$above 2 mHz and
(6 ± 1) x 10 fm s^{-2}/Hz$^{0.5}$ at 20 μHz

Predictions of the solar cycles 25-26

LISA-PF launch

LISA launch

We're here now

Fig. 5 Monthly variations of the observed and predicted (dotted) values of the sunspot numbers, F10.7 cm index and Lyman alpha index

Singh & Bhargawa Astrophys. Space Sci. (2019) 364:12
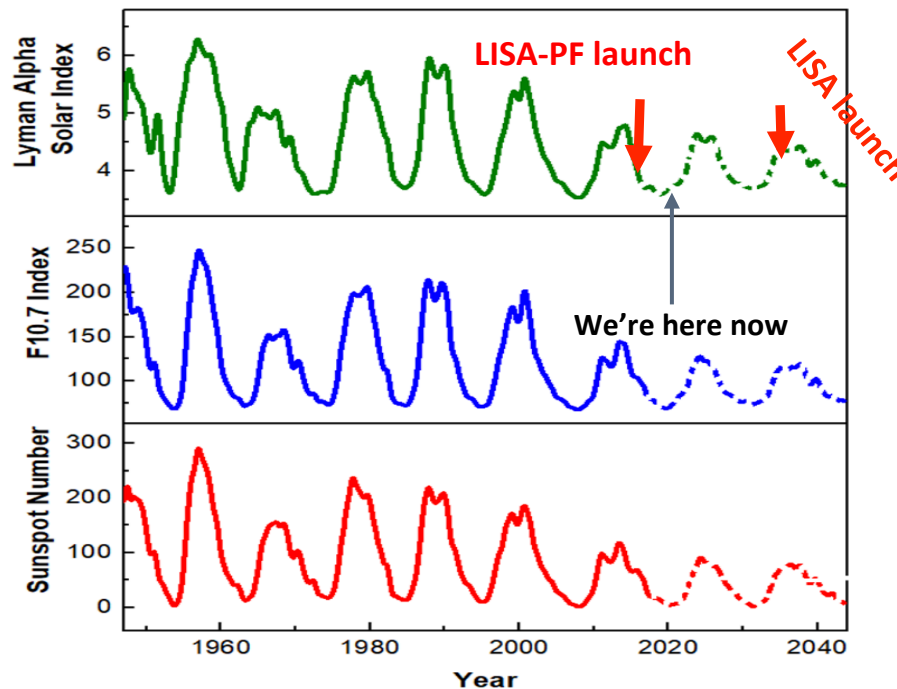
From the analysis of:

Ly-α index
F10.7 cm
Sunspot number
recorded in the last 70 years

In agreement with:
Cameron, Jiang and
Schussler
Apj, 823, L22, 2016
for the solar cycle 25

Cosmic-ray flux prediction and interpolation

Gleeson and Axford, Ap. J., 154, 1011, 1968

$$\frac{J(r,E,t)}{E^2-E_o^2} = \frac{J(\infty,E+\Phi)}{(E+\Phi)^2-E_o^2}$$

$\Phi_{m\_LISA}=200$ MV/c
$\Phi_{M\_LISA}=1200$ MV/c

$\Phi_{m\_LPF}=320$ MV/c
$\Phi_{M\_LPF}=550$ MV/c

J: particle flux

r: distance from Sun

E: particle total energy

t: time

E_o= particle mass

$\Phi= Ze\phi$ particle energy loss from ISM (different for each particle species)

$$F(E) = A\ (E+b)^{-\alpha}\ E^{\beta} \quad \text{particles } (\text{m}^2 \text{ sr s GeV n}^{-1})^{-1},$$

Papini, Grimani and Stephens, Nuovo Cimento, 1996

Φ from
http://cosmicrays.oulu.fi/phi/Phi_mon.txt

$$J_p(\infty,E+\Phi)$$

Burger, R. A., Potgieter, M. S. and Heber, B., JGR, 105, 27447, 2000

LISA Pathfinder monthly cosmic-ray observations

The LISA PATHFINDER mission
Orbit: L1 in 2016-2017

International sunspot number S_n : last 13 years and forecasts
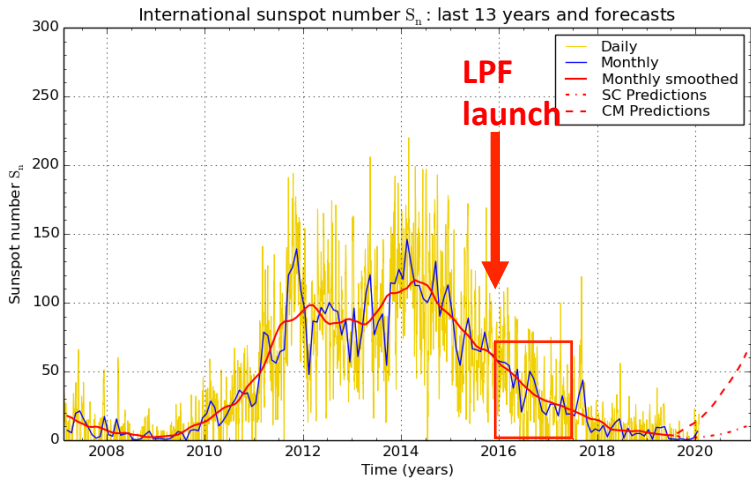
SILSO graphics (http://sidc.be/silso) Royal Observatory of Belgium 2020 February 1
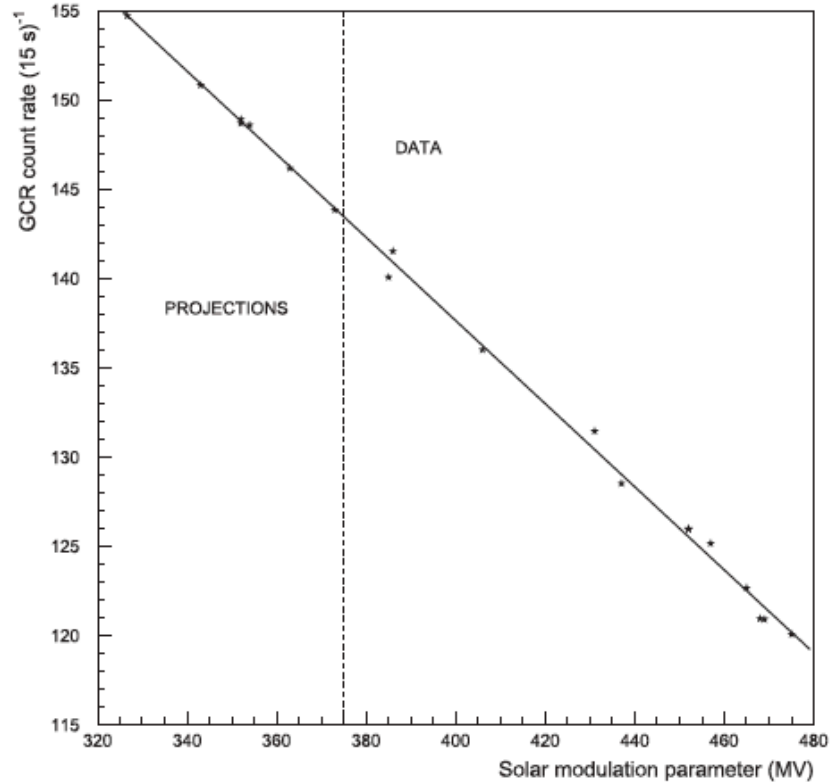
2015	695	686	743	705	655	666	617	612	611	601	585	561	644
2016	500	468	475	468	464	447	464	438	436	407	385	386	444
2017	366	357	348	367	359	350	383	420	444	405	367	360	377

http://cosmicrays.oulu.fi/phi/Phi_mon.txt

Monthly and daily solar modulation in 2016-2017: lessons learned with LISA Pathfinder

Armano et al.; ApJ,854, 113, 2018

Armano et al.; ApJ,874, 167, 2019
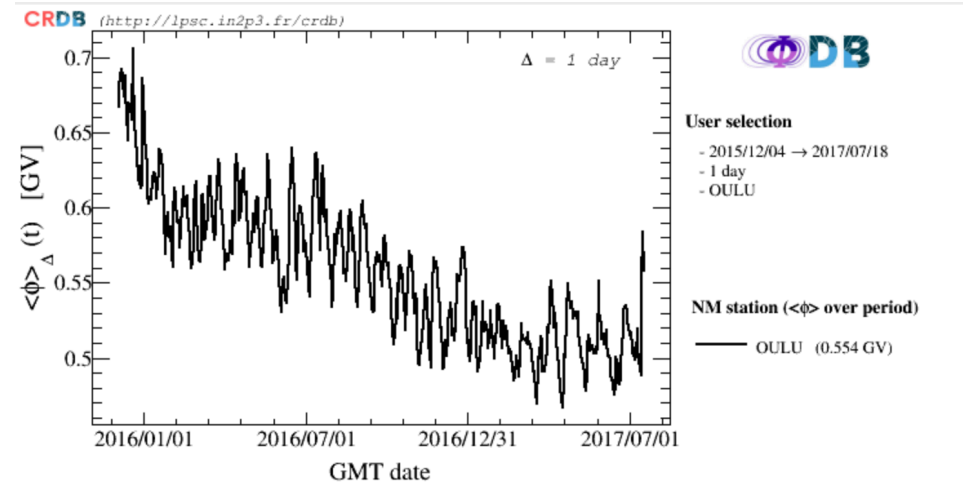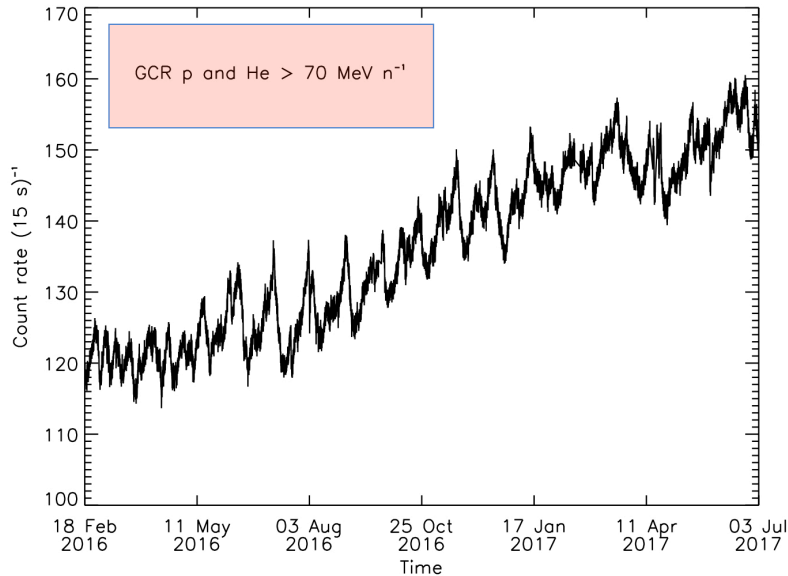
Increasing trend (decreasing solar modulation)

45 galactic cosmic-ray short-term recurrent depressions > 2 days

3 Forbush decreases

23 galactic cosmic-ray short-term non-recurrent variations < 2 days

Cosmic-ray short-term variations with LISA Pathfinder

Forbush Decreases
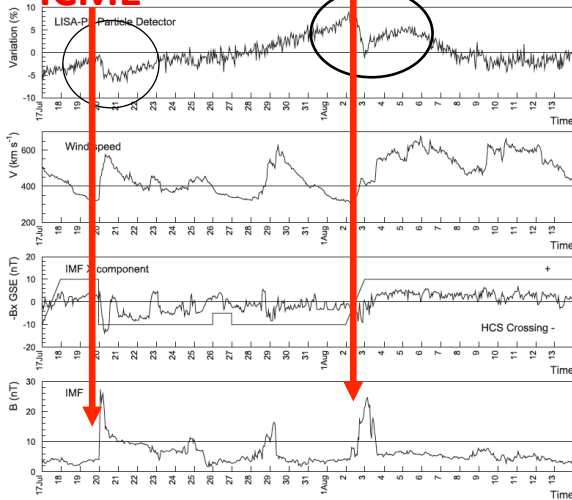
Recurrent galactic cosmic-ray flux variations

ICME

HSS

Bartels rotation 2496

Bartels rotation 2500

Bartels rotation 2501

ICME

Armano et al.; ApJ,854, 113, 2018
Armano et al.; ApJ,874, 167, 2019
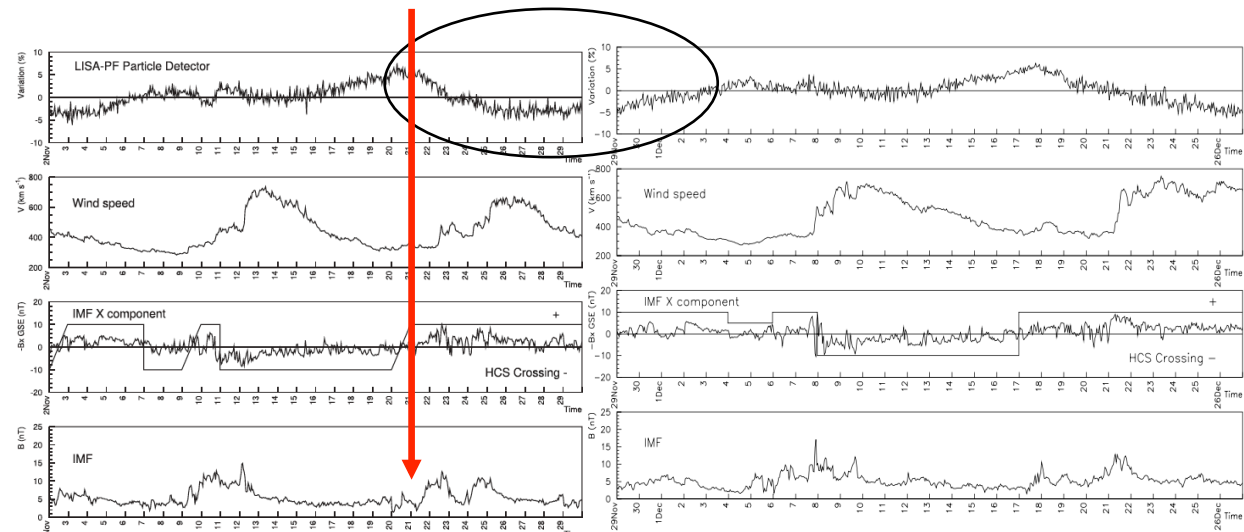
CG et al.; ApJ, 904, 64, 2020

Energy-dependence of galactic cosmic-ray long and short-term variations

Recurrent variations

Forbush decrease

Pred. 323 MV/c dotted
Obs: 383 MV/c
continuous

468 MV/c
Obs.: Dot-dashed

BARTELS Rotation 2509
Model prediction
BARTELS Rotation 2490
Model prediction

★ AMS experiment BARTELS Rotation 2490
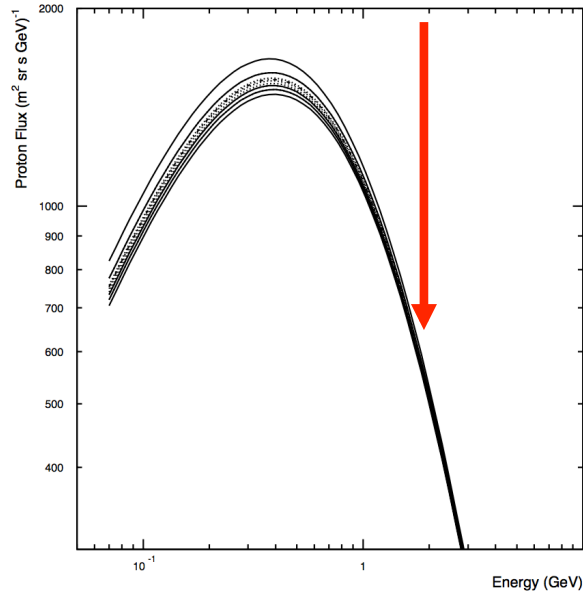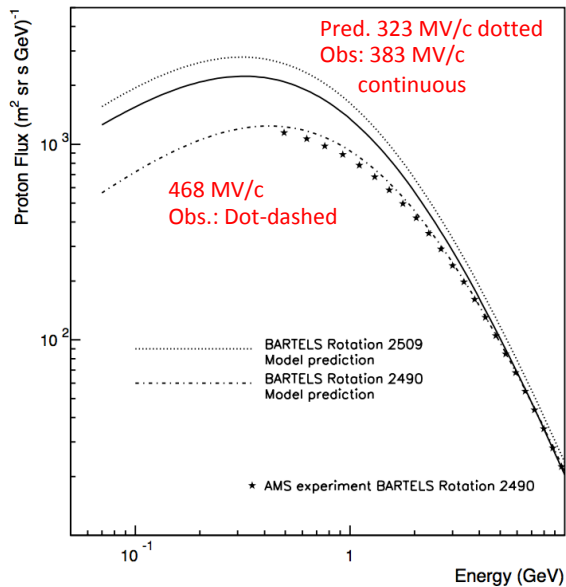
Fokker-Planck approach to reproduce galactic cosmic-ray short-term variations
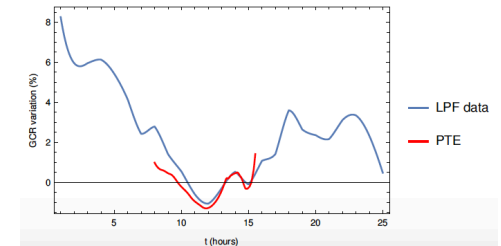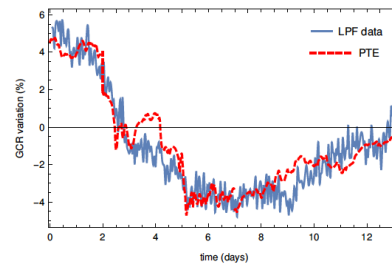
The PAMELA December 14, 2006 Forbush decrease

Onset

Mid main phase

Legend:
- 2016 August
- 2016 August 2 22.40 UT – LPF
- 2006 November – PAMELA
- 2006 December 14 – PAMELA 16.50–22.35 UT

Thule Neutron Monitor

Oulu Neutron Monitor

Rome Neutron Monitor

Mexico Neutron Monitor

7% depression on polar NMs

Onset November 2006
Net charging: 26.0 +e s^{-1}
Effective charging: 1169 e s^{-1}
Mid main phase December 14, 2006 17.20 UT
Net charging: 10.2 +e s^{-1}
Effective charging: 536.7 e s^{-1}
Dip December 15, 2006 00.00 UT
Net charging: 6.7 +e s^{-1}
Effective charging: 483.4 e s^{-1}

ESA ITT 10081

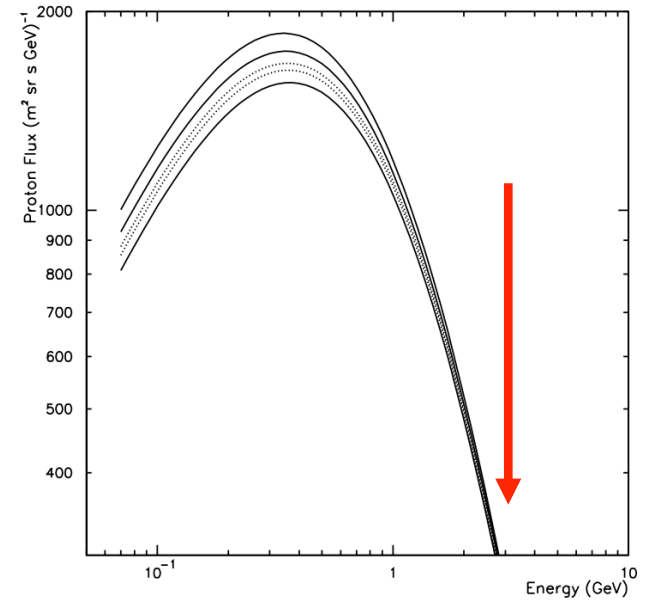48% depression In space

Onset

Mid main phase

Dip
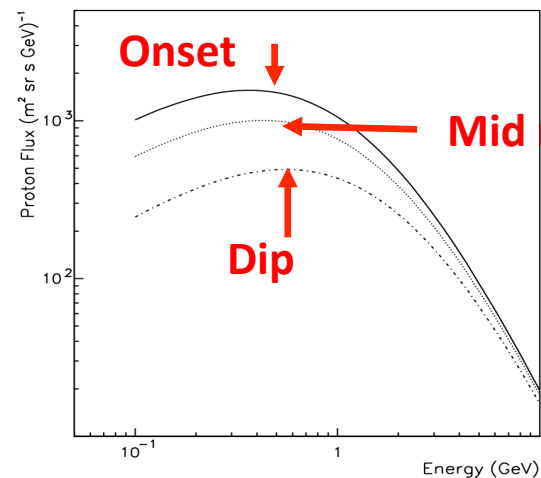
Adriani et al. 2011, ApJ, 742, 102
CG et al.; ApJ, 904, 64, 2020

Solar Orbiter and Metis

Antonucci et al., A&A 642 (A10), 2020
Romoli et al.;
https://www.aanda.org/articles/aa/pdf/forth/
aa40930-21.pdf

SoloHI

SWA-HIS

EPD-SIS

STIX

MAG-IBS

EUI

RPW-SCM

METIS

MAG-OBS

PHI

SWA-EAS

SWA-PAS

VL DETECTOR

1.2 g cm⁻² of shielding material

RPW-ANT

UV DETECTOR

MONTE CARLO MODEL
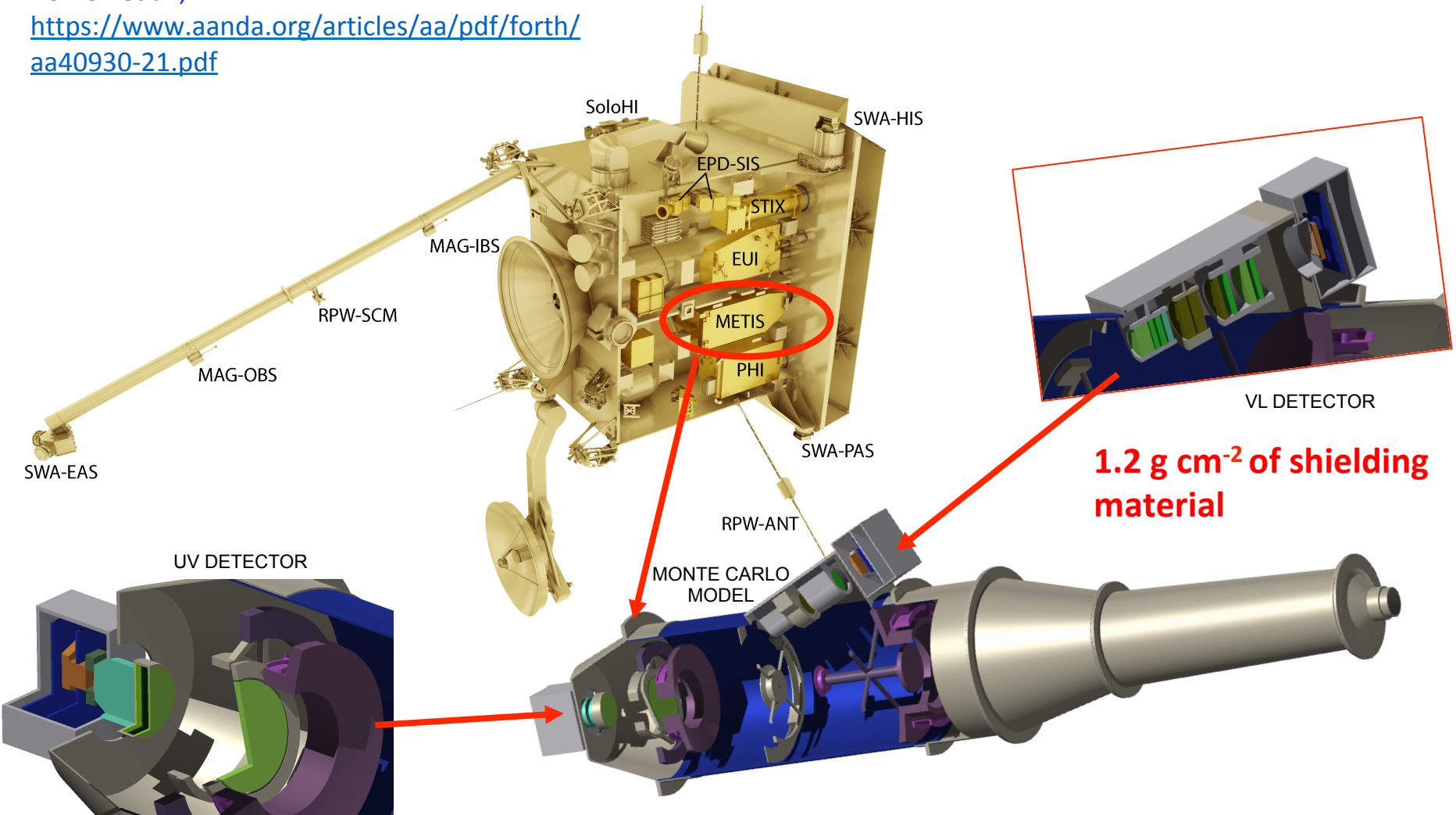
Cosmic-ray tracks in the Metis VL detector

λ= 580 – 640 nm

Metis/VL 15-May-2020 11:35:34.047
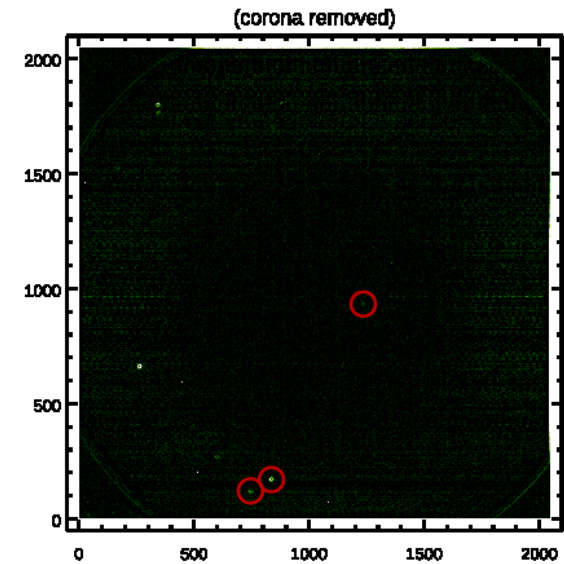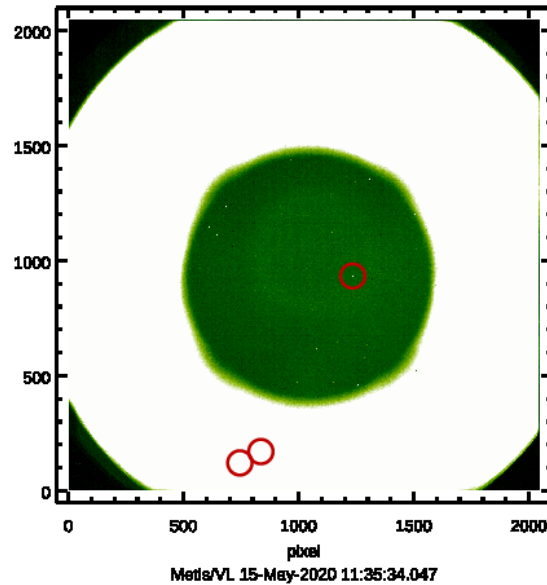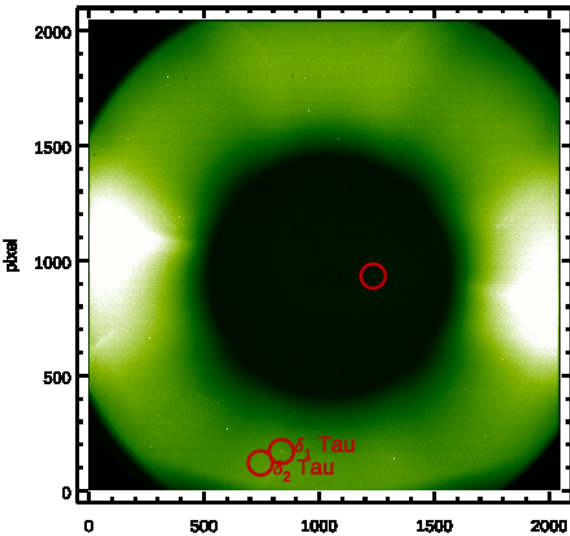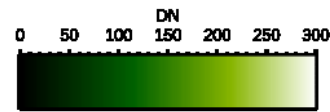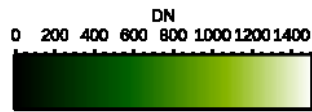
Courtesy of V. Andretta

The APviewer for cosmic-ray analysis in the Metis VL images

Single track
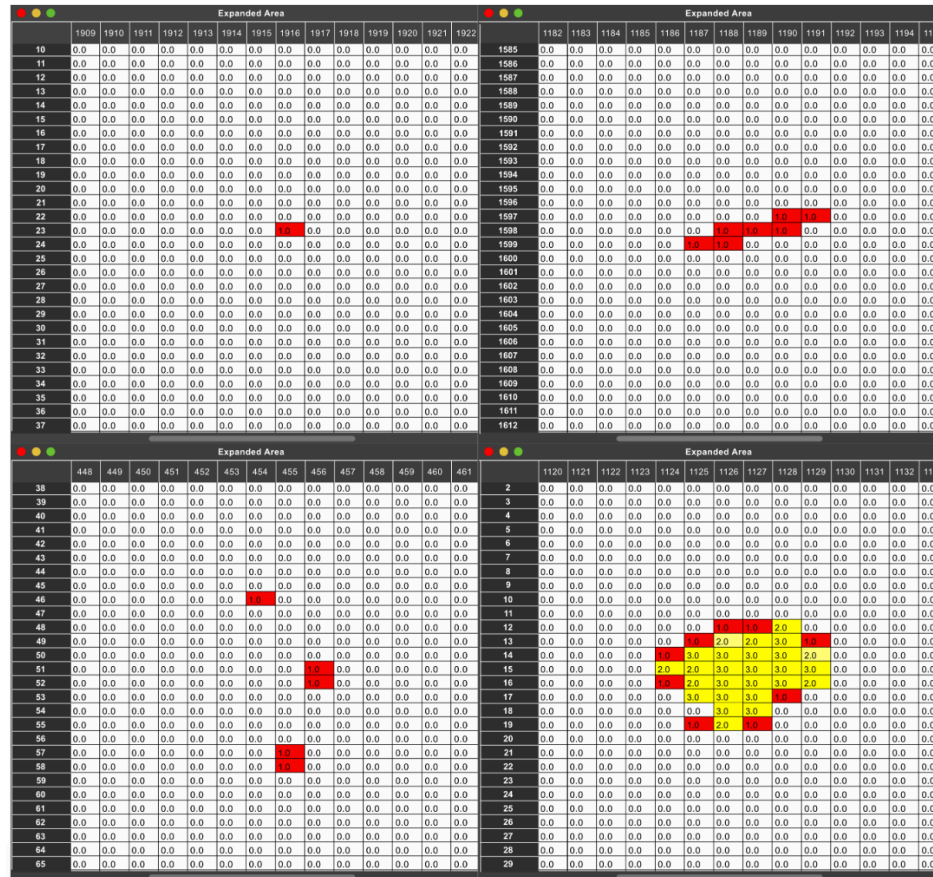
Single slant track

Multiple tracks

No cosmic ray

Persici A., University of Urbino Carlo Bo Thesis, 2021

METIS MONTE CARLO SIMULATIONS WITH FLUKA

FLUKA FLAIR SolO SIMULATION GEOMETRY

CG et al.;
https://arxiv.org/abs/2104.13700
https://www.aanda.org/articles/aa/pdf/forth/aa40930-21.pdf
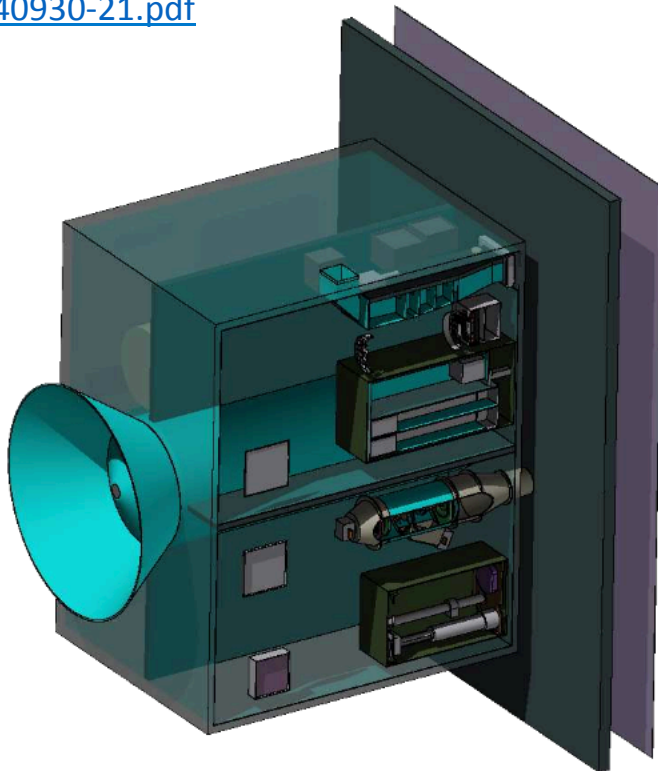
← **EUI**

← **METIS**

← **PHI**

FLUKA SIMULATION OUTCOMES:

- **Approximately 50% of incident protons are stopped in the spacecraft material surrounding Metis**
- **The spurious pixels fired by cosmic rays are 10^{-4} of the total sample in the VL detector**
- **The multiple tracks are not secondaries**
- **The observed number of tracks is compatible with primary and secondary particles generated by protons only (IMP!!!)**
- **Metis may play the role of a proton monitor**

Thanks to the PHI and EUI Collaborations

Circumpulsar/magnetar disc formation

- Coplanar planets surround the millisecond pulsar PSR 1257+12 (Wolszczan & Frail 1992)

- A fallback disc was detected around the anomalous X-ray pulsar (AXP) 4U 0142+61 (Wang, Chakrabarty & Kaplan 2006)

- The presence of a disc around the RRAT B0656+14 was reported in Perna, Hernquist & Narayan (2000). In Grimani (2013) it was pointed out that a precessing disc would have explained the transient emission from this pulsar

- The hypothesis of a disc surrounding Crab just beyond the LC was discussed in Menou, Perna & Hernquist (2001)

- The presence of a disc may be responsible of pulsar spin down

- The presence of a disc may also affect high-energy electron and positron propagation in the pulsar and magnetar near environment

The case of the AXP 4U 0142+61

- In addition to the disc around the AXP 4U 0142+61 detected by Spitzer (Wang, Chakrabarty & Kaplan 2006; Ertan et al. 2007)…

- …**the Nuclear Spectroscopic Telescope Array (NuSTAR) experiment detected an X-ray emission modulated at 55 ks, or half this value, from the same AXP (Makishima et al. 2018).**

- It is shown here that this modulation is compatible with the presence of a Keplerian precessing disc with the characteristics observed by Wang et al. (2006) hiding periodically the emission region.

Characteristics of AXP 4U 0142+61

- Mass: 2.8×10^{30} kg

- Radius: 10 km

- Period: 8.68917 s

- Magnetic field: $(4.75 +/- 0.02) \times 10^{14}$ G

- Blackbody temperature: 3.59×10^6 K

- Blackbody radiation: 0.309 +/- 0.001 keV

- Distance from Earth: 3.6 kpc

- Momentum of inertia: 1.12×10^{38} kg m^2

- Angular momentum: 8.10×10^{37} kg m^2 s^{-1}

Characteristics of the disc around AXP 4U 0142+61

- Inner radius (R_I): 2.02×10^9 m

- Outer radius (R_o): 6.75×10^9 m

- Disc height: $0.035\ R_I$

- Mass: 5.97×10^{25} kg

- Blackbody Temperature: 920 K

- Blackbody $\lambda_{max} = 3.15 \times 10^{-6}$ m (mid-infrared)

- Disc temperature compatible with 5% absorption of the magnetar illuminating energy

- Momentum of inertia: $I_D = 1.48 \times 10^{45}$ kg m^2

- Angular momentum: $L_D = 2.23 \times 10^{41}$ kg m^2 s^{-1}
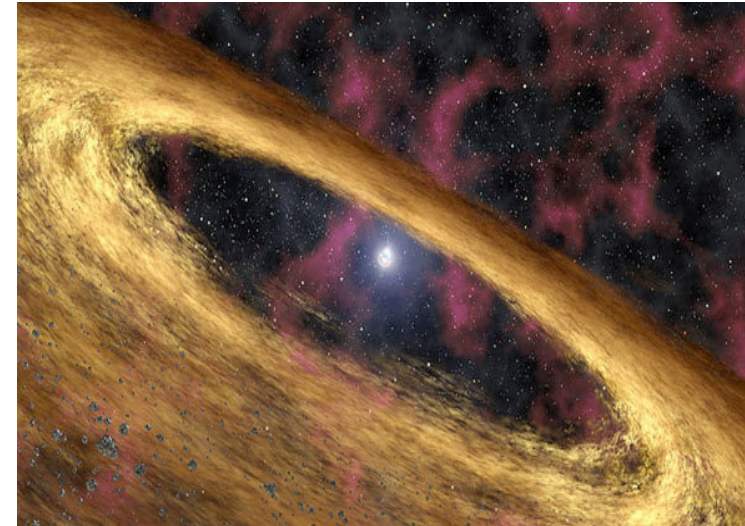
Pulsed photon observations from Crab with MAGIC
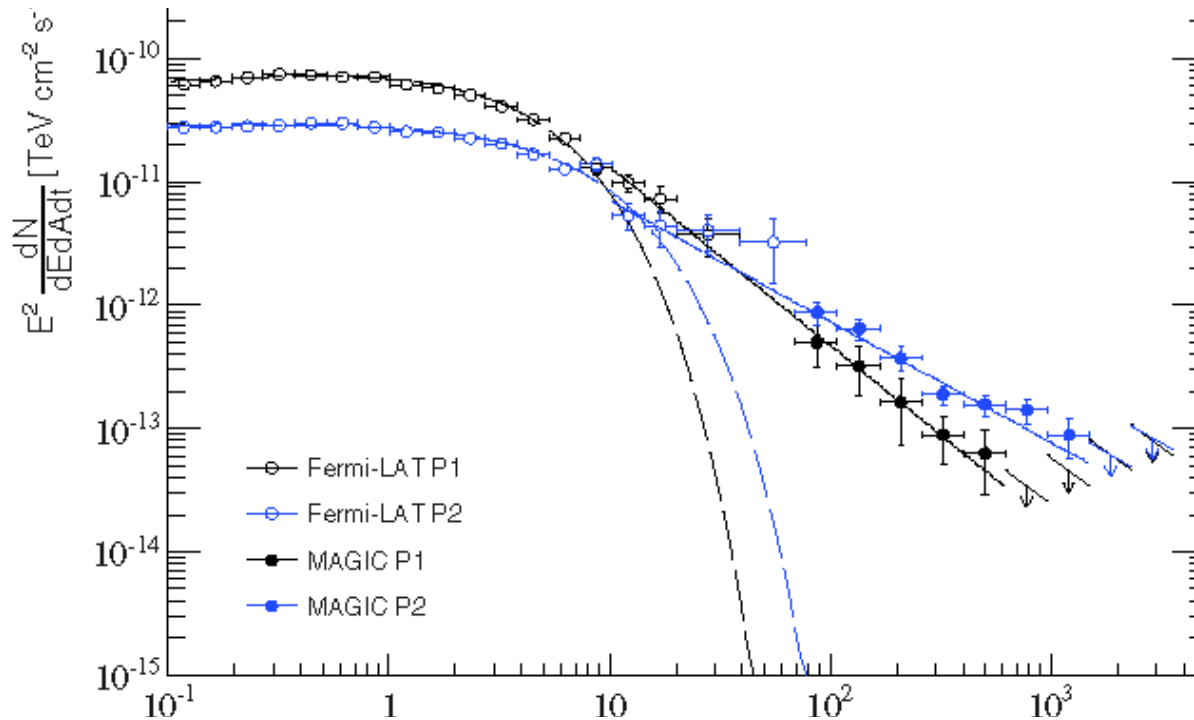
Ansoldi et al., A &A, 585, A133 (2016)

IC scattering dominates above 50 GeV. Aharonian et al. suggested this takes place at 50-60 light cylinder radius distance (10^7-10^8 m; when measurements were available up to 400 GeV): may infrared emission from a disc possibly contribute in limiting the propagation of TeV electrons and positrons?

James Webb Space Telescope

- The James Webb Space Telescope (JWST; Gardner et al. 2006), scheduled to launch in December 2021, will definitely open the infrared observational window on disc formation around magnetars and pulsars.
- Gravitational wave emission from precessing discs may also help in detecting these discs

4U 0142+61: disc precession or magnetar precession forced by the disc?

- The NuSTAR observations are compatible with a precessing Keplerian disc

- Keplerian frequency: $V = R_l \Omega_K$ $V = [(GM_{mag})/R_l]^{1/2}$

- $V = 3.0 \times 10^5$ m s^{-1} and $\Omega_K = 1.505 \times 10^{-4}$ s^{-1}

- $\omega_{mag} = 0.723$ s^{-1}

- $P = 2\pi/\phi$ with $\phi = (45\ M_D \cos \theta'\ \omega_{mag})/(32\ \pi\ \rho\ R_l^3)$

  Tong *et al* 2020 *Res. Astron. Astrophys.* **20** 142

  where $\theta' = 15^o$, $\rho = 10^{17}$ kg m^{-3} for the NS density with

  θ' representing the angle formed by the rotation axis of the

  magnetar and the perpendicular to the disc plane

  $P = 2.77 \times 10^{20}$ s different from NuSTAR observations: this scenario

  would work only for heavy discs formed near young pulsars

May be a free magnetar precession?

The magnetar free precession would imply a magnetic field of the magnetar of 10^{16} G (Makishima et al.; 2018) that however, is not in agreement with observations: (4.75 +/- 0.02)x10^{14} G (Guver et al., 2008)

Gravitational wave emission from precessing discs

Table 1. Gravitational wave amplitude generated by precessing discs and detection distances for $\theta = 10°$. The signal-to-noise ratio (S/N) is inferred from the *LISA* (below 10^{-3} Hz) and *BBO* (above 10^{-3} Hz) sensitivities reported in Fig. 2. Maximum distances for precessing disc detection, when feasible, are set for S/N = 1. The detection probability would increase with the square root of the observational time.

	Disc mass (kg)	$\omega_1(\omega_2)$ (Hz)	$h_{\omega_1}(h_{\omega_2})$	$S/N_{\omega_1}(S/N_{\omega_2})$	Distance (kpc)
4U 0142+61	5.97×10^{25}	$3.1 \times 10^{-4}(6.2 \times 10^{-4})$	$1.1 \times 10^{-26}(4.5 \times 10^{-26})$	$\ll 1(\ll 1)$	0.05(0.05)
Crab	5.97×10^{25}	$3.9 \times 10^{-2}(7.8 \times 10^{-2})$	$6.7 \times 10^{-26}(2.7 \times 10^{-25})$	$\ll 1(<1)$	0.05(0.05)
	10^{27}	$3.9 \times 10^{-2}(7.8 \times 10^{-2})$	$1.1 \times 10^{-24}(4.5 \times 10^{-25})$	$<1(1)$	0.05(0.5)
	10^{28}	$3.9 \times 10^{-2}(7.8 \times 10^{-2})$	$9.3 \times 10^{-25}(4.8 \times 10^{-25})$	$1(1)$	0.6(4.65)
	10^{29}	$3.9 \times 10^{-2}(7.8 \times 10^{-2})$	$8.7 \times 10^{-25}(4.5 \times 10^{-25})$	$1(1)$	6.8(50.0)

Table 2. Same as Table 1, but for $\theta = 30°$. For masses of 10^{29} kg, in principle, disc precession detection may extend to the whole Galaxy (WG).

	Disc mass (kg)	$\omega_1(\omega_2)$ (Hz)	$h_{\omega_1}(h_{\omega_2})$	$S/N_{\omega_1}(S/N_{\omega_2})$	Distance (kpc)
4U 0142+61	5.97×10^{25}	$3.5 \times 10^{-4}(7.0 \times 10^{-4})$	$1.9 \times 10^{-25}(4.8 \times 10^{-25})$	$\ll 1(\ll 1)$	0.05(0.05)
Crab	5.97×10^{25}	$4.4 \times 10^{-2}(8.8 \times 10^{-2})$	$7.2 \times 10^{-25}(4.8 \times 10^{-25})$	$1(1)$	0.05(0.3)
	10^{27}	$4.4 \times 10^{-2}(8.8 \times 10^{-2})$	$8.0 \times 10^{-25}(4.2 \times 10^{-25})$	$1(1)$	0.75(5.7)
	10^{28}	$4.4 \times 10^{-2}(8.8 \times 10^{-2})$	$8.1 \times 10^{-25}(4.2 \times 10^{-25})$	$1(1)$	7.5(57.1)
	10^{29}	$4.4 \times 10^{-2}(8.8 \times 10^{-2})$	$7.1 \times 10^{-25}(4.1 \times 10^{-25})$	$1(1)$	84.5(WG)

CG, CQG, 2009; CG Adv. Sp. Res. 2013; CG MNRAS, 2016; CG MNRAS, 2021

Electron and positron propagation in the region of the disc formation

- Blackbody photon density near a disc:
- $N/V = 8\,\pi\,(kT/hc) \times 2.405$

  with $V = 1$ cm^3 $T = 920$ K $N = 1.57 \times 10^{10}$ photons cm^{-3}

  and $T = 1800$ K $N = 1.18 \times 10^{11}$ photons cm^{-3}

- Average energy is 0.21 eV and 0.43 eV, respectively, in the near infrared region

- Pulsar blackbody radiation: $N = 1.15 \times 10^9$ photons cm^{-3}

- The infrared radiation emission is approximately one order of magnitude smaller than that of the disc (Penny 1982)

Discs that may limit the propagation of TeV electrons and positrons

Klein-Nishina total cross section

$$\sigma_{KN} = \sigma_T \frac{3}{4} \left[\frac{1+x}{x^3} \left(\frac{2x(1+x)}{1+2x} - \ln(1+2x) \right) + \frac{1}{2x} \ln(1+2x) \right. $$

$$\left. + -\frac{1+3x}{(1+2x)^2} \right], \qquad (19)$$

where $x = h\nu_o/(m_e c^2)$. Since $h\nu_o/(m_e c^2) > 1$ the above equation can be reduced as follows:

$$\sigma_{KN} = \sigma_T \frac{3}{8} \frac{1}{x} \left(\ln 2x + \frac{1}{2} \right). \qquad (20)$$

Where $h\nu_o$ is the maximum photon energy in the electron rest frame

The total cross section and associated collision length is 9.9×10^{-30} m^2 and 8.6×10^{11} m. Only discs of a.u. dimensions and hundreds of degrees temperature may limit the propagation of TeV electrons and positrons.
This is the case of the XTIN J0806.44123 for instance.

Conclusions

- Any astrophysical source being possibly at the origin of the positron excess in cosmic rays should be properly considered before evaluating the role of exotic sources

- Interplanetary physics of cosmic rays may give a major contribution to space weather science and mission diagnostics

- Fallback matter and disc formation near pulsars and magnetars may limit the maximum energy of electrons and positrons reaching the inner heliosphere

- Direct observations of discs through infrared emission are expected to be allowed by JWST. Future gravitational wave detection from precessing discs may help in solving the puzzle in the whole Galaxy